The South Pacific Convergence Zone in three decades of satellite images

Colene Haffke[1] and Gudrun Magnusdottir[1]

Received 1 April 2013; revised 28 August 2013; accepted 13 September 2013; published 4 October 2013.

[1] Interannual variability, seasonal evolution, and intraseasonal variability of the South Pacific Convergence Zone (SPCZ) are quantified using a new data set of 3-hourly SPCZ labels, available from 1980 to 2012 Nov–Apr. The SPCZ label is a binary field indicating presence (1) or absence (0) of the SPCZ at each grid point (½° longitude by ½° latitude) as a function of time and is the output of a Bayesian spatiotemporal statistical model that takes in instantaneous data from geostationary satellites. The statistical model is designed to emulate the way human observers identify the SPCZ. Results show two distinct parts to the SPCZ: the western tropical part and the eastern subtropical part. At times, the two parts do not connect. When they do connect, they are oriented quite differently, such that the subtropical part has a steeper meridional slope. The SPCZ is present 50–70% of the time in the tropics from Jan to Mar and is usually anchored to the warm sea surface temperature (SST) distribution of the equatorial west Pacific. The subtropical part does not have the same sensitivity to the underlying SST distribution and is present more often in Nov–Dec and Apr than in Jan–Mar when the SST is highest. Interannual variability in SPCZ location is strongly associated with El Niño–Southern Oscillation (ENSO); however, no change in overall SPCZ area is detected in association with ENSO. On the intraseasonal time scale, composite analysis shows the distinct spatial patterns in SPCZ presence associated with each phase of the Madden Julian Oscillation.

Citation: Haffke, C., and G. Magnusdottir (2013), The South Pacific Convergence Zone in three decades of satellite images, *J. Geophys. Res. Atmos.*, *118*, 10,839–10,849, doi:10.1002/jgrd.50838.

1. Introduction

[2] The South Pacific Convergence Zone (SPCZ) is an elongated convection zone that is easily recognizable from space, especially during the austral summer half-year (Nov–Apr). In monthly or seasonal averages, and sometimes instantaneously, it is located on a path stretching from the equatorial region near New Guinea in the west (near 140°E) to the subtropics near 30°S, 120°W in the east [e.g., *Vincent*, 1994]. The tilt in latitude makes the SPCZ different from other elongated tropical convergence zones such as the east Pacific Intertropical Convergence Zone (ITCZ), which is active north of the equator, especially during boreal summer [*Bain et al*., 2011]. Part of the SPCZ is located within the deep tropics, part is located in the subtropics, and part occasionally stretches into the extratropics in the east, with dynamical processes in each region playing a role in SPCZ formation and maintenance. The exact location of the SPCZ controls the distribution of precipitation and any severe weather since, true to any tropical convergence zone, cyclogenesis takes place on the poleward side of the tropical portion of the SPCZ [*Gray*, 1979; *Jourdain et al*., 2011, *Vincent et al*., 2011, *Lorrey et al*., 2012].

[3] The orientation and extent of the SPCZ have been attributed to various processes such as the following: (1) control from a tropical heat source over the maritime continent and a forced equatorial Rossby wave response in the Southern Hemisphere [*Matthews et al*., 1996], (2) the interaction of subtropical flow, resulting from a tropical heat-source forcing, and the mean extratropical flow southwest of the SPCZ [*Kodama*, 1999, and references therein], and (3) eddy forcing from the extratropics [e.g., *Matthews*, 2012, *Widlanski et al*., 2011, and references therein]. *Takahashi and Battisti* [2007] present convincing evidence, using a coupled global climate model, that the Andes play a major role in setting up the dry zone bounding the SPCZ in the equatorial direction, thus providing a complementary viewpoint. While blocking the westerlies, the Andes force a subsiding equatorward flow on the windward side, leading to evaporative cooling, low sea surface temperatures (SST), and stratus clouds in the southeast Pacific. The diagonal shape of the SPCZ is associated with streamlines of the southeasterly trades in this wedge-shaped, precipitation-free area. *Lintner and Neelin* [2008] confirmed in observations that high-frequency wind variations of the inflow in the dry zone determine the eastern extent of the SPCZ.

[4] Previous observational studies have primarily focused on describing the mean state of the SPCZ in terms of cloud

Additional supporting information may be found in the online version of this article.

[1]Department of Earth System Science, University of California, Irvine, California, USA.

Corresponding author: C. Haffke, Department of Earth System Science, University of California, Irvine, CA 92697-3100, USA. (chaffke@uci.edu)

2169-897X/13/10.1002/jgrd.50838

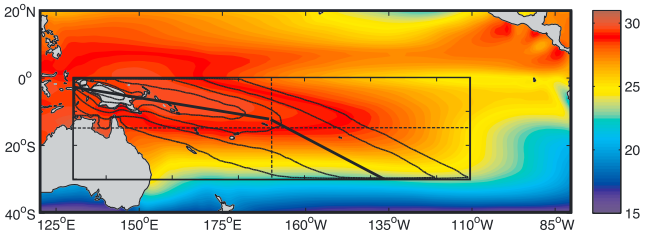

Figure 1. The domain for this study spans 0–30°S, 130° E–110°W, and is outlined by the smaller black box. SPCZ fraction of time present for the 1980–2011 austral summer half-year (Nov–Apr) is shown in black contours starting at 10% in intervals of 10%. The years 1987 and 1988 are excluded. Shading shows mean SST (°C) from 1982 to 2012 over the austral summer half-year. Dashed black lines split domain into quadrants and the two bold black lines show the main axis of the 30 year mean SPCZ.

and/or rainfall location, and describing interannual variability, especially variability in SPCZ location associated with the El Niño Southern Oscillation (ENSO). The SPCZ shifts to the north during El Niño years, becoming more zonally oriented like a typical tropical convergence zone such as the east Pacific ITCZ [e.g., *Bain et al*., 2011]. During La Niña years, it shifts southwest from its mean location [*Folland et al*., 2002]. *Vincent et al*. [2011] recently showed that the SPCZ response to ENSO is slightly more complicated. They examined a 24 year (1979–2002) record in ERA40 reanalysis and in rainfall data from the Global Precipitation Climatology Project (GPCP). Three out of seven El Niño events during their record show a zonally oriented tropical SPCZ, the rest exhibiting a northward shift without the zonal alignment. Three ENSO neutral years in their study also show a northward shift of the SPCZ.

[5] In this study we will quantify interannual and intraseasonal variability in SPCZ location and area using a 3-hourly data set of SPCZ presence. SPCZ presence labels are generated by adapting and applying the Markov Random Field (MRF) spatiotemporal statistical model originally developed by *Bain et al*. [2011] to identify the east Pacific ITCZ. The statistical model has a built-in tendency to clump together observations of SPCZ presence in space and time, emulating the way a human would recognize this meteorological feature. By automating the method, more data may be processed and the results are independent of human judgment so that the same results are always obtained given the same raw data, which may not be the case for human analysis [*Bain et al*., 2011, *Henke et al*., 2012]. The model can accept multiple forms of input data at one time but we will concentrate on showing results based on the atmospheric window infrared channel (IR) from the GridSat database [*Knapp et al*., 2011] as it gives a 30 year record of variability in cloudiness. SPCZ presence labels are also created using total precipitable water (TPW) and the visible channel (VS) from the GridSat database in addition to IR input, but this resulted in a much shorter record of only 15 years. The SPCZ labels produced using TPS, VS, and IR input are not significantly different from the IR-only input labels. In past studies, IR-only labels were used to study the diurnal cycle of the east Pacific ITCZ [*Bain et al*., 2010] as well as its interannual variability [*Bain et al*., 2011].

[6] This data set of SPCZ labels is unique in that it gives the location and outline of the instantaneous SPCZ every 3 h from which the total area or cloud top height distribution within the SPCZ can be calculated, for example. Likewise, composite analysis based on certain climate indices, such as the MJO, can be performed. To our knowledge this technique has not been used before as previous studies have relied on averages, mostly of precipitation, over a certain time period, such as a month or a season. However, instantaneous fields of precipitation are noisy and even when thresholding outgoing longwave radiation (OLR) or the IR channel used here, the results are also quite noisy in instantaneous data (see discussion in *Bain et al*. [2011]).

[7] This paper is organized as follows: Section 2 describes data and methods. Section 3 contains results on the mean SPCZ and its variability in terms of interannual variability of the SPCZ in 3.1, in terms of seasonal evolution in 3.2 and in terms of intraseasonal variability associated with the MJO in section 3.3. Section 4 contains concluding remarks.

2. Data and Methods

2.1. Satellite Data

[8] In this study we take the SPCZ to represent a convection zone as seen in cloud fields or outgoing longwave radiation from the IR atmospheric window channel in the GridSat data set. GridSat is a recently archived collection of geostationary satellite images with global, long-term coverage appropriate for climate studies [*Knapp et al*., 2011]. Measurements originally brought together as part of the ISCCP B1 archive from geostationary satellites (from the U.S., Europe, Japan, and China) have been intercalibrated and stitched together to form the data set. IR images are available every 3 h from 1980 to 2012 at 8 km spatial resolution. To improve efficiency of the statistical model, the IR data was coarsened to 0.5° spatial resolution.

2.2. SPCZ Labels

[9] The 3-hourly data set of SPCZ location consists of binary labels designating the presence/absence of the SPCZ for each grid point in a 0.5° × 0.5° gridded IR satellite image. The domain of study extends from the equator to 30°S and from 130°E to 110°W as shown in Figure 1. The SPCZ labels are available every 3 h during the austral summer half-year.

[10] The labels are generated by a Markov random field statistical model, using IR data as input. The model calculates the probability of SPCZ presence at each grid point and classifies points as SPCZ if the probability is greater than 0.5. This ensures that grid points that are more likely to be SPCZ than non-SPCZ are included in the SPCZ label. Results are not sensitive to the threshold of 0.5 because a large majority of grid points have probabilities of being SPCZ that are near to zero or one. The probabilities depend on the following factors: The likelihood (via Bayes rule) of the observed IR value at the grid point, the presence/absence of SPCZ at neighboring grid points in space and time, and the location of the grid point in the domain. The dependence on neighboring grid points introduces a recursive aspect to the computation, and the location term ensures that unrelated features are not identified as being part of the SPCZ. The technique of Gibbs sampling [*Geman and Geman*, 1984; *Gilks et al*., 1996] is used to stochastically search for high-probability

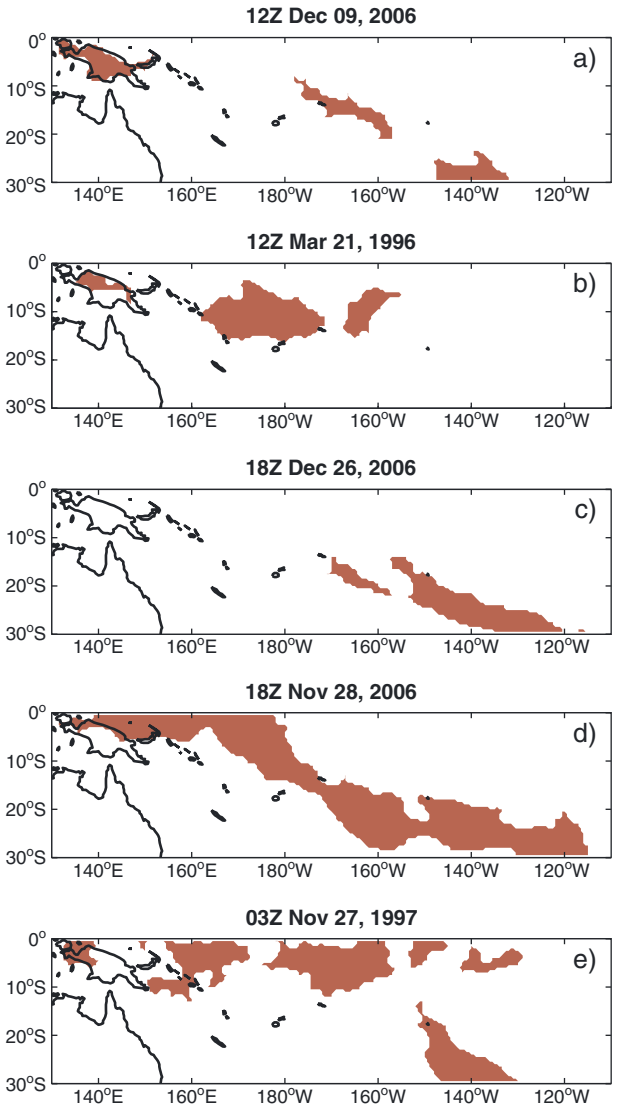

Figure 2. Examples of instantaneous SPCZ binary labels created by the spatiotemporal statistical model. The five dates are chosen to demonstrate the model's ability to capture the SPCZs varied location.

assignments of each grid point to SPCZ presence/absence, given the observed IR data. Smooth, continuous regions of SPCZ are identified by this method. Full details of the model as applied to the east Pacific ITCZ are given by *Bain et al.* [2011]. The only difference in the statistical model as applied to the SPCZ is that the spatial prior that was zonally symmetric for the ITCZ with a Gaussian distribution in latitude is tilted in latitude for the SPCZ with the same Gaussian distribution off the tilted line [see *Bain et al.* [2011, Figure 2b]. To retrain the model, three meteorologists manually outlined the SPCZ in a 1 month subset (January 2001) of 3-hourly IR images to obtain the likelihood of the observed IR values for SPCZ versus non-SPCZ grid points. *Bain et al.* [2011] found that this statistical method provided systematic improvement in labeling accuracy over other automated techniques when compared to human labelers. The statistical method was also more consistent with other automated techniques than they were with each other. Figure 2 shows five different examples of instantaneous SPCZ labels produced by the statistical model, demonstrating its ability to handle very different SPCZ configurations. In particular, Figure 2e shows how the model is able to capture the equatorward shift of the SPCZ in an El Niño year.

[11] As mentioned previously, an additional data set of SPCZ labels was created using VS, TPW, and IR as input to the statistical model. The VS and TPW data are only available since 1995 and this resulted in a shorter time series of SPCZ presence. Climatology based on SPCZ labels using all three inputs were broadly in line with climatology based on the longer time series of IR-only labels. SPCZ labels created using all three inputs were more inclusive than IR-only SPCZ labels north of 25°S and slightly less inclusive south of this latitude; however, there was little difference in the location of the labels. Results in this paper therefore focus on the IR-only labels. We will also note that no attempt was made to separate out tropical cyclone convection from the SPCZ labels although the connection between the location of the SPCZ and tropical cyclone development has been noted [e.g., *Diamond et al.*, 2013; *Lorrey et al.*, 2012; *Jourdain et al.*, 2011].

[12] The 3-hourly SPCZ labels are produced for Nov–Apr from 1980 to 2012 except for the 1987 and 1988 seasons when large gaps exist in the raw satellite data. This study is limited to the austral summer half-year as the SPCZ is less active in austral winter. The following analysis will make use of the absolute spatial extent of the SPCZ label as a proxy for SPCZ area. The frequency of occurrence of SPCZ at a particular grid point refers to relative frequency of the label being equal to 1 at that location.

2.3. SPCZ Axis Lines

[13] Mean SPCZ location and extent can be quantified by compositing the SPCZ labels over different periods of time, giving the fraction of time the SPCZ is present in any location. The mean location and orientation will be described by the main axis of the mean SPCZ, consisting of two line segments, one representing the tropical SPCZ, and the other representing the subtropical SPCZ. Although the model was designed to identify the SPCZ as one continuous, elongated convective zone, stretching from the tropics to the subtropics, most often the mean SPCZ naturally segments into two linear parts that have different slopes (see contours in the figure in section 3.2, for example). The tropical portion is usually more zonally oriented and is present more often during the active season, while the subtropical portion has a steeper slope, or steeper angle of incidence into the subtropics, and is more spatially variable.

[14] The following steps are used to create the two lines describing the main axis of the mean SPCZ. First, the SPCZ binary labels (SPCZ or non-SPCZ) are composited over a given time period (one season, for example), which produces a mean SPCZ with units of fraction of time present. Next, the locations of maximum fraction of time present are found. For each longitude in the domain, there will be one latitudinal location where the SPCZ fraction of time present is maximum, resulting in 241 latitude, longitude grid points of maximum SPCZ fraction of time present. One line is fit through the western portion of these points to describe the tropical SPCZ and a second line is fit through the eastern portion to describe the subtropical SPCZ. If the maximum fraction of time present is located at 30°S, all points to the

east of this point are not included in the calculation of the eastern line. Two methods were used to determine the longitudinal segmentation between the grid points describing the tropical SPCZ and those describing the subtropical SPCZ, one automatic and one manual. For the automatic method, the error between the grid points of the maximum SPCZ fraction of time present and the two lines representing the SPCZ is minimized by changing the longitude of the segmentation point. We found that this method produced useful results most of the time; however, for some years the fraction of time present pattern was such that this method segmented the SPCZ in a way that did not support our goal of describing the tropical and subtropical segments. For example, the automatic method would segment the SPCZ too far west, creating a "subtropical SPCZ" that stretched all the way to the equator and a "tropical SPCZ" that spanned a short distance to the western boundary. Due to this discrepancy, we also performed a manual method of segmenting the two lines by making a visual inspection of the SPCZ fraction of time present plot to determine the longitude where the tropical and subtropical SPCZ naturally segments. The automatic method works well for the 30 year mean SPCZ (Figure 1) and monthly mean SPCZ (see figure in section 3.2), but the manual method was necessary for seasonal mean SPCZ (see Figure S1 in the supporting information).

2.4. Grouping Patterns of Interannual Variability

[15] To characterize SPCZ interannual variability, we develop a method that groups seasons based on the spatial pattern of SPCZ presence anomalies. To create SPCZ presence anomalies, we first take a 30 year average of SPCZ labels at each 3 h time step, forming the mean seasonal cycle, and then we subtract the seasonal cycle from each time step in all 30 years. The time series of SPCZ presence anomalies is then used to make a composite for each season. Using the composites, SPCZ anomalies are averaged over latitudes equatorward of the main axis of the 30 year mean SPCZ (see Figure 1) as a function of longitude. This specific metric is chosen because it concisely captures the changes in SPCZ behavior throughout the entire domain. Three variables can describe the shape of our metric as a function of longitude: (1) the mean SPCZ presence anomaly at 130°E (the westernmost point), (2) the longitude at which the mean anomaly reaches an extremum in the central part of the domain, and (3) the value of the mean anomaly at that longitude. Seasons with similar values for these three variables are grouped together, creating a total of eight groups. Although we do not consider ENSO mode in our method, seasons with the same ENSO mode are generally grouped together, with several exceptions.

2.5. Additional Data Used in Analysis

[16] SPCZ location will be compared to the underlying SST. Monthly mean SST is obtained from the NOAA Optimum Interpolated SST V2 data set [*Reynolds et al*., 2002] at a 1.0° × 1.0° resolution for the years 1982 through 2012, Nov–Apr. This data set is a combination of in situ and satellite measurements. The SST data is provided by the NOAA/OAR/ESRL PSD, Boulder, Colorado, USA, from their Web site at http://www.esrl.noaa.gov/psd/. The SST data is interpolated onto a 0.5° × 0.5° grid for comparison to SPCZ labels.

[17] SPCZ activity is examined with respect to MJO phase in section 3.3. MJO phase and amplitude data are described in *Wheeler and Hendon* [2004] and downloaded from cawcr.gov.au/staff/mwheeler/maproom/RMM/. This data set lists the MJO phase and amplitude for each day since 1974. Only days with an MJO amplitude greater than 1 are used.

[18] Finally, SPCZ activity is also examined with respect to ENSO mode. The Multivariate ENSO Index (MEI) is used to define the state of ENSO [*Wolter and Timlin*, 1998]. Bimonthly MEI values are downloaded from http://www.esrl.noaa.gov/psd/people/klaus.wolter/MEI/mei.html. To determine the ENSO state for each SPCZ active season, an average MEI value is calculated from the Nov/Dec, Dec/Jan, Jan/Feb, Feb/Mar, and Mar/Apr bimonthly periods. Oct/Nov and Apr/May are not included in the calculation to reduce the influence from months that are outside the austral summer half-year. The average MEI value determines which seasons are classified as El Niño seasons ($MEI > 0.5$), La Niña seasons ($MEI < -0.5$), and ENSO neutral seasons ($-0.5 < MEI < 0.5$). Using this categorization method. El Niño years include 1982, 1986, 1987, 1991, 1992, 1994, 1997, 2002, 2004, and 2009, La Niña years include 1984, 1988, 1995, 1998, 1999, 2000, 2005, 2007, 2008, 2010, and 2011, and ENSO neutral years include 1980, 1981, 1983, 1985, 1989, 1990, 1993, 1996, 2001, 2003, and 2006.

3. Results and Analysis

[19] Examples of instantaneous, 3-hourly SPCZ labels, shown in Figure 2, highlight the variable nature of SPCZ extent and location. At times the SPCZ is fragmented, consisting of several unconnected pieces that, together, span the length of the domain (Figure 2a). At other times the SPCZ is active only in the tropics (Figure 2b), or the subtropics (Figure 2c). Sometimes, the SPCZ exists as one complete feature, stretching from the tropics to the subtropics without any segmentation (Figure 2d). Individual labels can appear in the tropics and then propagate along the length of the SPCZ axis or they can appear and disappear in one location, indicating the varied nature of convection within the SPCZ. The SPCZ mean state is defined by a composite of all SPCZ labels from 1980 to 2012 during the austral summer half-year (Nov–Apr). Black contours in Figure 1 indicate the fraction of time the SPCZ is present in each location in the domain. Throughout the paper we will also use the phrase "SPCZ activity" to refer to SPCZ fraction of time present. The two bold black lines show the location of the main axis of the 30 year mean SPCZ and are created using the automatic method described in section 2.3. The SPCZ is most active in the tropics near Papua New Guinea, where it is present 50% to 70% of the time in the 30 year average. SPCZ activity decreases to the east and south and is present less than 30% of the time in the subtropics. The shading in Figure 1 shows the mean SST for Nov–Apr in the years 1982 to 2012 over a region including and extending beyond the domain used for SPCZ detection. North of the equator, the location of the ITCZ is associated with the band of maximum SST and the strong SST gradient [Xie, 2005]. Similar to the ITCZ in boreal summer [*Bain et al*. 2011], the tropical part of the SPCZ in Figure 1 is anchored to the high SST in the west Pacific warm pool. The subtropical

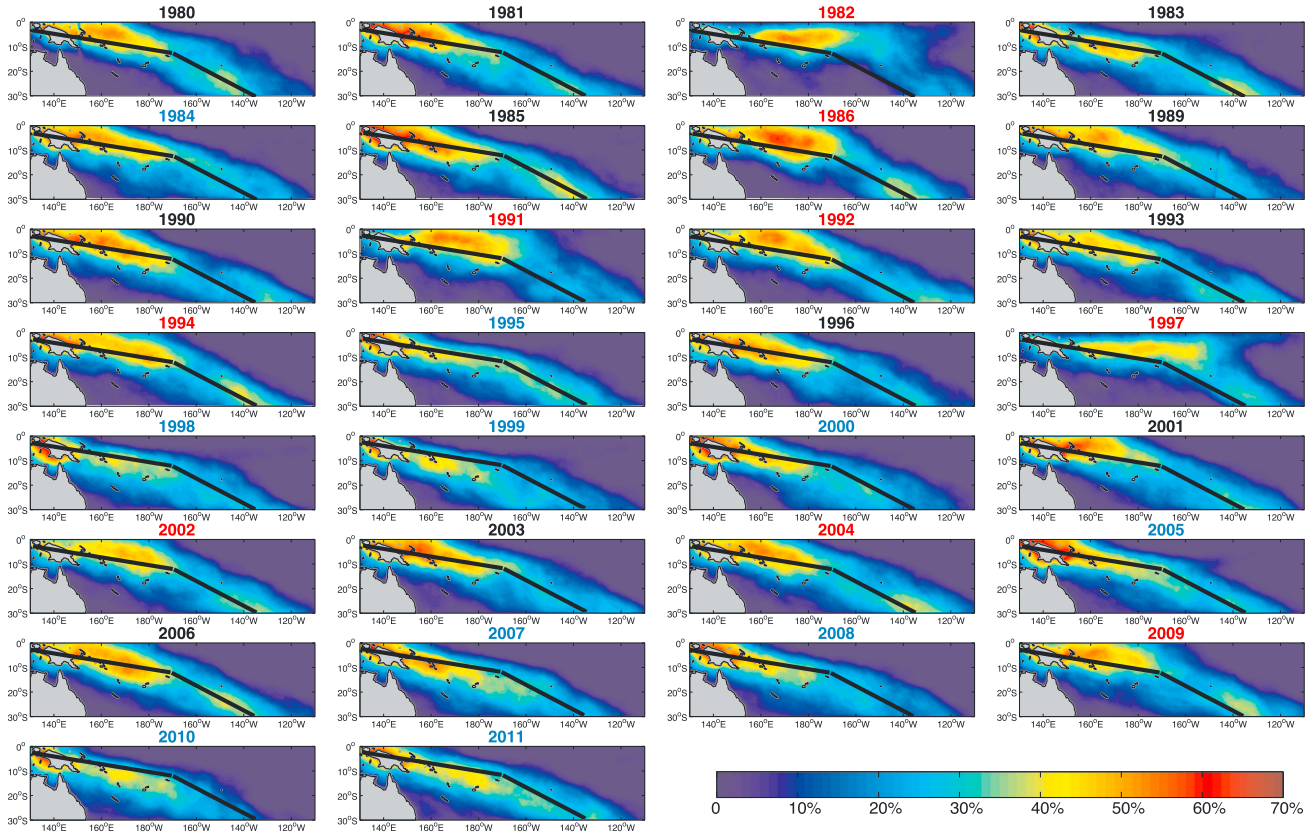

Figure 3. SPCZ fraction of time present for each austral summer half year (Nov–Apr). Panel titled 1980 represents Nov 1980 through Apr 1981. Panel titles are color coded by ENSO mode: El Niño seasons (MEI > 0.5) (red), La Niña seasons (MEI < -0.5) (blue), and ENSO neutral seasons ($-0.5 <$ MEI < 0.5) (black). Bold black lines are the same for each panel and show the main axis of the 30 year mean SPCZ.

SPCZ deviates from the pattern of high SST. Even though there is some tilt in latitude of the high SST pattern going from west to east, this tilt is far less pronounced than the tilt in SPCZ location east of the dateline.

3.1. Interannual Variability of the SPCZ

[20] From the binary SPCZ labels, we obtain 30 years of SPCZ presence from 1980 to 2011, excluding 1987 and 1988. Figure 3 shows the fraction of time the SPCZ is present, as well as two bold lines indicating the main axis of the 30 year mean SPCZ (also shown in Figure 1), for each austral summer half-year. The pattern of SPCZ presence changes from year to year, indicating variability in the location of SPCZ labels. Despite the variability from year to year, common spatial patterns emerge when seasons are compared. For example, 1986, 1991, and 1992 all show a northward shift in SPCZ location compared to the 30 year mean, while 1998, 1999, and 2011 all have a southward shift. Past studies describe how interannual variability of SPCZ position is dominated by ENSO [e.g., *Folland et al.* 2002; *Vincent et al.* 2011]. In El Niño years, the SPCZ shifts equatorward and east, such as in 1982. The opposite occurs in La Niña years when the SPCZ shifts poleward and west, such as in 1999. To better describe interannual variability, we use the method described in section 2.4 to represent the continuum of behavior with respect to the mean location shown in Figure 1. The method, which does not rely on categorization according to ENSO, results in eight groups, each describing a unique spatial pattern of SPCZ presence.

[21] The eight groups are presented in Figure 4. The curves represent the spatial pattern of the SPCZ anomalies north of the main axis of the 30 year mean SPCZ for each season. As group number increases from one to eight, SPCZ anomalies north of the 30 year main axis get more positive. Groups 1, 2, and 3 have mostly negative anomalies north of the main axis line, and as the group number increases, the area of the negative anomaly decreases and shifts to the east. Groups 4–8 have mostly positive anomalies north of the main axis line, and as the group number increases, the area of the positive anomaly increases and shifts east.

[22] Although not explicitly accounted for, seasons with the same ENSO mode are typically grouped together. The eight groups provide more detail about variability in SPCZ behavior within years belonging to the same ENSO mode. Group 1 is composed of the first (2010), third (1998), and fourth (1999) strongest La Niña seasons as indicated by average MEI value. Seasons in this group have a strong negative SPCZ anomaly north of the mean axis line and a fairly strong positive anomaly south of the main axis line indicating a shift in SPCZ location to the southwest. Group 2 comprises six La Niña seasons, including the strongest (2007), and one ENSO neutral season (1983). The SPCZ also shifts to the southwest for Group 2, but the shift is not as great as for Group 1.

[23] An inspection of the two ENSO neutral seasons in Group 3 (1981 and 1985) suggests a concentration of SPCZ

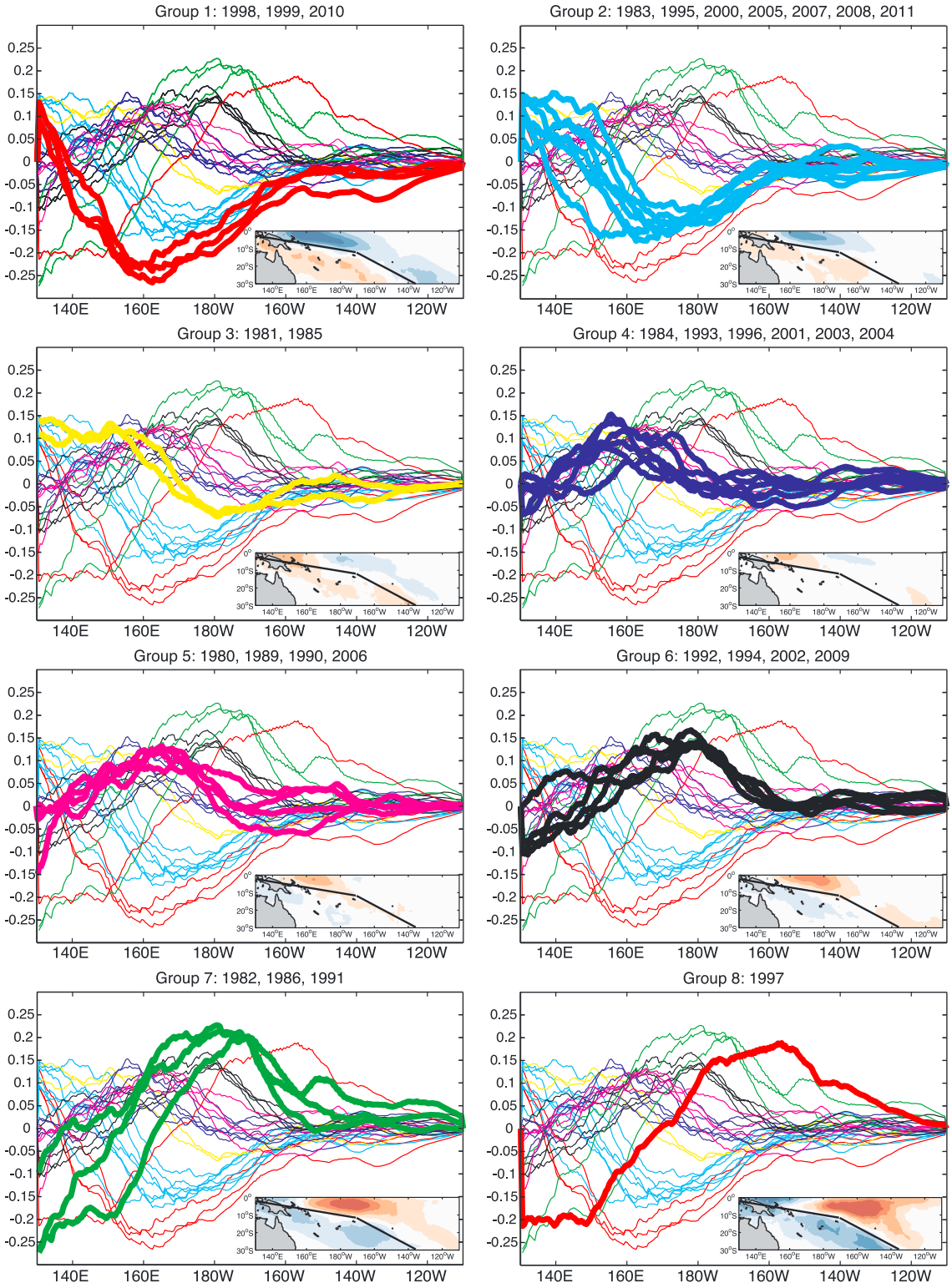

Figure 4. Each panel describes one of eight groups used to categorize SPCZ interannual spatial variability. The title for each panel lists the group number and all seasons belonging to that group. Curves show the mean fraction of time present (after seasonal cycle has been removed) north of the main axis of the 30 year mean SPCZ as a function of longitude. Curves for the group being described are shown in bold in each panel. Smaller inset panels show the fraction of time present with the seasonal cycle removed over all seasons belonging to that group. Blue shading represents locations where the SPCZ is less frequently present than the mean, while red shading shows areas where the SPCZ is more frequently present than the mean. Contours start at 3% (−3%) and are at intervals of 6% (−6%). Two bold black lines in the smaller inset panels show the main axis of the 30 year mean SPCZ.

Table 1. Mean Slope Values and Segmentation Points During Different States of ENSO[a]

	Slope of Western SPCZ (°latitude/°longitude)	Slope of Eastern SPCZ (°latitude/°longitude)	Longitude of Segmentation
ENSO Neutral	0.18 (0.04)	0.46 (0.08)	160°W (6°)
La Niña	0.23 (0.04)	0.38 (0.24)	163°W (10°)
El Niño	0.14 (0.04)	0.45 (0.23)	155°W (8°)

[a]Standard deviations are shown in parentheses.

activity in the west as opposed to a shift in SPCZ location as seen in Groups 1 and 2. A similar, but weaker pattern is evident in Groups 4 and 5. Group 5 contains only ENSO neutral seasons while Group 4 contains one El Niño season (2004) and one La Niña season (1984), in addition to four ENSO neutral seasons. While 2004 is the weakest El Niño season with an MEI value 0.662, 1984 is not the weakest La Niña season as 2005, 2000, and 1995 all have less negative MEI values (closer to the cutoff of −0.5). On average, seasons in Groups 4 and 5 do not show strong positive or negative anomalies indicating these seasons have a SPCZ fraction of time present pattern that is close to the overall mean.

[24] Group 6 contains the next four weakest El Niño seasons after 2004. The anomaly pattern for seasons in Group 6 is more indicative of a shift to the northeast than that seen in Group 5. A strong northeastward shift is indicated by the spatial pattern for seasons in Group 7, which contains the first (1982), third (1991), and fourth (1986) strongest El Niño years. Group 8 only consists of one season, 1997, which is the second strongest El Niño season.

[25] Again, the eight groups generally follow ENSO mode, but they also capture subtle differences in the location and strength of the shifting SPCZ. *Vincent et al*. [2011] categorize interannual SPCZ location into four classes (asymmetric, positive, neural, and negative). When comparing the classes defined in *Vincent et al*. [2011] to the eight groups, we find that they mostly agree. For example, all seasons in Groups 1 and 2 are classified as negative, but Groups 4 and 5 are split between neutral and positive classes. Although 1982, 1991, and 1997 are all classified as asymmetric in *Vincent et al*. [2011], we find that 1982 and 1991, as well as 1986, belong to Group 7 while only 1997 belongs to Group 8.

[26] ENSO mode strongly influences SPCZ location, but we find that it does not strongly influence total SPCZ area. The mean area (not shown) during each season is calculated over the entire domain as well as for each of the four regions shown by dashed lines in Figure 1. Area is calculated by summing all grid points included in the SPCZ labels. Mean annual SPCZ area in the northeast (southwest) region is highly correlated (anticorrelated) with the annual mean MEI (0.84 and −0.90, respectively). This arises because the SPCZ typically shifts into the northeast region during El Niño years and into the southwest region in La Niña years. SPCZ area in the northwest and southeast regions, where the SPCZ is most present, are not correlated with MEI, having correlation coefficients of 0.21 and −0.04, respectively. Thus, mean SPCZ area over the entire domain is not strongly correlated with MEI on an interannual time scale, having a correlation coefficient of 0.35. The top five seasons by SPCZ area are as follows: 1985, 1989, 2004, 2009, and 1984. Two ENSO neutral seasons, two El Niño seasons, and one La Niña season, respectively. All top five seasons by area belong to Groups 3–6, groups that have the smallest SPCZ anomalies. The five seasons with the smallest SPCZ area are as follows: 2010, 1999, 1980, 1982, and 1988. The year 1980 is an ENSO neutral year, 1982 is an El Niño year, and the other three are La Niña years. Groups 1 and 7 have strong SPCZ anomalies and four out of the five seasons with the smallest SPCZ area are in these groups. Six out of nine El Niño years fall within the top half of seasons by area, while eight out of 10 La Niña seasons fall within the bottom half.

[27] The orientation of the SPCZ also changes depending on ENSO mode. Table 1 summarizes the mean slopes of the main axis of the seasonal mean SPCZ (slopes shown in Figure S1 in the supporting information), as well as the mean longitude of segmentation between the two portions during ENSO neutral, La Niña, and El Niño years. During El Niño years, the tropical portion of the SPCZ becomes more zonal as compared to ENSO neutral years. During La Niña years, the opposite is true; the slope of the tropical SPCZ becomes steeper. The segmentation of the SPCZ also changes with ENSO mode. In El Niño years, the tropical segment of the SPCZ stretches further to the east and during La Niña years the tropical segment is shorter, being cut off further to the west. The mean longitude of segmentation during El Niño years is at 155°W and during La Niña years is at 163°W.

3.2. Seasonal Evolution of the SPCZ

[28] To describe the seasonal evolution, SPCZ labels are used to calculate area and the fraction of time the SPCZ is present. For each month, Figure 5 shows the composite of SPCZ labels over all years (contours) plotted with the mean SST for each month from 1982 to 2012 (shading). Two bold black lines in each panel indicate the main axis of the mean SPCZ for that month and are created by the method described in section 2.3. Figure 5 shows how the SPCZ fraction of time present evolves throughout the season and how this evolution is different in the tropics (north of 15°S and west of 160°W) than in the subtropics (south of 20°S and east of 160°W).

[29] Figure 6 shows the mean SPCZ area for each 3-hourly time step. Fractional area covered by the SPCZ is calculated by summing all points within the SPCZ label at every 3 h time step within each region, and then averaging over all years. The domain is split into four quadrants, each extending over 15° in latitude and 60° in longitude. Dashed lines in Figure 1 outline the quadrant. The northwest quadrant (130°E–170°W, 0–15°S) and the southeast quadrant (170°W–110°W, 15°S–30°S) are used to describe SPCZ area since they capture the majority of SPCZ activity. The thick black curves in Figure 6 show the 7 day running mean of SPCZ area for each region. The highest frequency variability is due to the diurnal cycle, which shows up clearly in both regions in terms of SPCZ area (see section 3.3 for a discussion of spectral analysis of the signal).

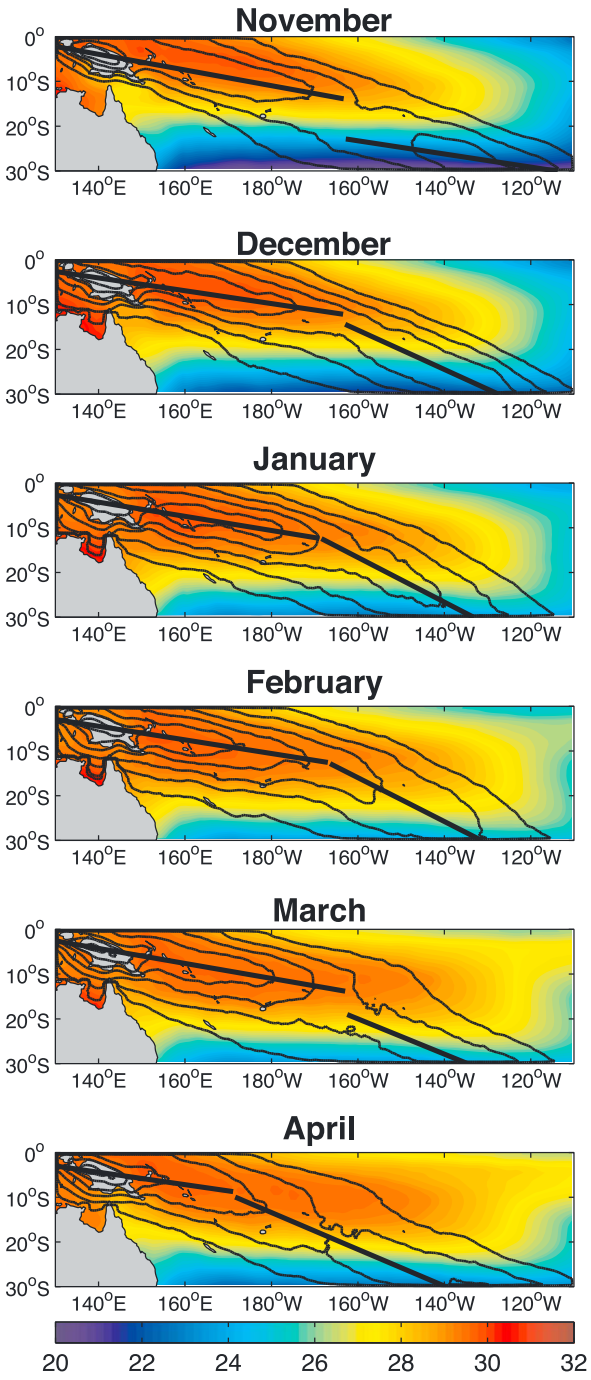

Figure 5. SPCZ fraction of time present for each month, over all seasons 1980–2011 (excluding 1987 and 1988) in black contours. Contours start at 10% and are at intervals of 10%. Shading shows mean SST (°C) for each month over all seasons 1982–2012. Bold black lines represent the main axis of the monthly mean SPCZ.

[30] Focusing first on the subtropics in Figure 5, the fraction of time the SPCZ is present is the highest in November and December (greater than 30%), indicating that the SPCZ is most active in this region early in the season. SPCZ area is also greatest in the subtropics in November and December, reaching maximum in late December (Figure 6). In November, the axis lines in Figure 5 do not meet, indicating that the SPCZ in the two regions is disconnected. During January, February, and most of March, SPCZ area in the subtropics gets smaller, reaching a minimum in late March. This is consistent with a decline in the fraction of time the SPCZ is present in the subtropics in Jan–Mar (Figure 5). In April there is a small region near the southern border of the domain where the SPCZ is present more than 30% of the time (Figure 5, bottom). SPCZ area in the subtropics also increases in April.

[31] In the tropics, the SPCZ is not as active in November as during the rest of the season. Activity picks up in December and by February the SPCZ is present 78% of the time at maximum. The maximum fraction of time present in each month can be found near 4°S, 139°E, over Papua New Guinea. Although the highest fraction of time present at any one point occurs in February, the SPCZ is most active over the largest area in January. During December, January, and February, the axis lines are connected, indicating activity occurring along a continuous path. In March, the SPCZ occurs less frequently in the tropics and in April SPCZ presence and area continue to decrease.

[32] Seasonal changes in the location of maximum SST in the east Pacific are accompanied by a similar change in maximum ITCZ fraction of time present (*Bain et al.*, 2011). As the maximum SST shifts north, so does the ITCZ, indicating that high SST and ITCZ position are closely linked. A similar relationship was not found for the subtropical SPCZ. From November to April, the warm pool expands to the east and south so that the coldest SST are located in the subtropics in November at the same time the SPCZ is most active in the same region. SST is warmest in the subtropics in February and March, a time when SPCZ activity in the subtropics is lowest.

[33] The variability in SPCZ fraction of time present described above represents a long-term mean, but the seasonal evolution could vary from year to year, for example, during different phases of ENSO. To examine this possibility, SPCZ monthly composites similar to those in Figure 5 are created for El Niño seasons only, La Niña season only, and

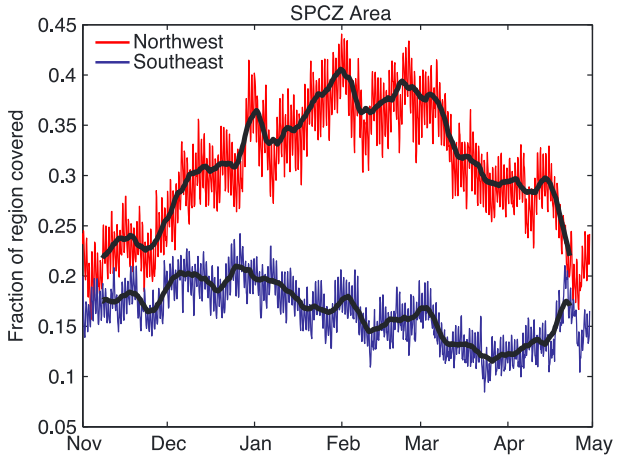

Figure 6. Mean SPCZ area over 1980–2011 seasons for the northwest (0–15°S, 130°E–170°W) and southeast (15°S–30°S, 170°W–110°W) regions in units of fraction of region covered. Red and blue curves show the 3-hourly areas while black curves show the 7 day running means.

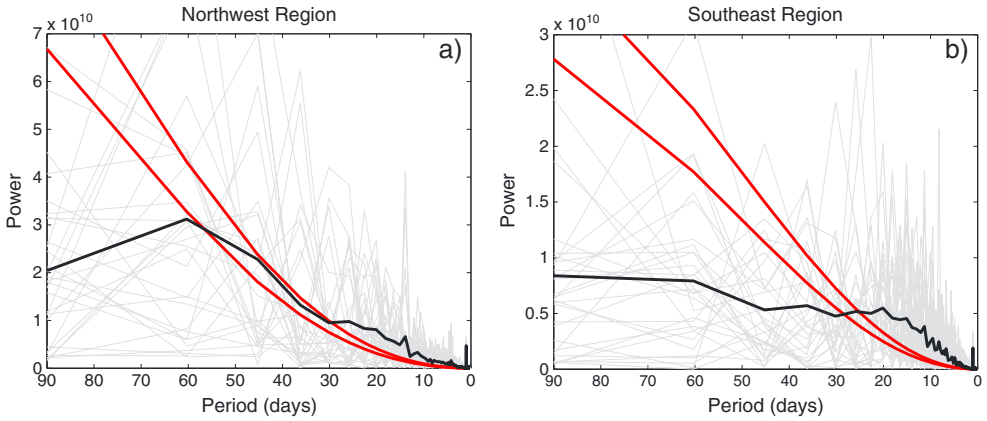

Figure 7. Solid black curve shows the power spectra for 3-hourly SPCZ area from 1980 to 2011 Nov–Apr for the northwest region and southeast region of the domain (see regions in Figure 1). Lower red curve is the red-noise spectra and upper red curve is the 95% confidence spectra. Light gray lines are the power spectra for the individual seasons (30 total).

ENSO neutral seasons only (Figure S2 in the supporting information). Seasons are categorized based on the method described in section 2.5. We do not find a difference in seasonal evolution as described above during different phases of ENSO. The subtropical SPCZ is still most active during November and December and the tropical SPCZ is most active in January and February. The biggest difference during El Niño years is an increase in SPCZ activity near the equator early in the season, starting in the beginning of November. In La Niña years, a large positive SPCZ anomaly is located north of Australia early in the season, starting at the end of November.

3.3. Intraseasonal Variability of the SPCZ

[34] Within any given year, there is intraseasonal variability in SPCZ area and location. Figures similar to Figure 6, but for each year individually (not shown), indicate a wide range of variability in SPCZ area. At times, the area of the tropical SPCZ will increase or decrease along with the area of the subtropical SPCZ, and at other times, the area in two regions will change independently. Figure 7a shows a power spectrum of 3-hourly SPCZ area in the northwest region and indicates peaks above the 95% confidence spectra for periods less than 30 days. The most significant peak occurs at 1 day and indicates a strong diurnal cycle in SPCZ area while a second peak occurs at 14 days. Figure 7b shows the same plot but for the southeast region. In the subtropics, spectral peaks in SPCZ area occur above the 95% confidence level for periods less than 22 days. Again, the largest peak occurs at 1 day.

[35] Past studies have noted that on the intraseasonal time scale, SPCZ location and intensity change during different phases of the MJO [*Matthews et al.*, 1996; *Matthews*, 2012]. The MJO is an atmospheric circulation pattern characterized by a region of enhanced convection, followed and preceded by a region of suppressed convection, which propagates eastward along the equator with a period of 30–60 days [*Madden and Julian*, 1993]. One way to describe the propagation of the MJO is by categorizing the location of enhanced convection. *Wheeler and Hendon* [2004] define an index which describes the strength and phase of the MJO daily from 1974 to the present. The index is based on the combined empirical orthogonal functions (EOF) of 850 hPa and 200 hPa zonal wind, along with OLR. *Matthews* [2012] finds that the MJO can modify the basic state to change the probability of occurrence of two modes of SPCZ variability that they identify: a SPCZ that is shifted southwestward and an enhanced SPCZ located in the typical location. Here we expand this description of the MJO-SPCZ relationship by providing the spatial patterns of SPCZ presence during each phase of the MJO. After removing the seasonal cycle from the 3-hourly SPCZ labels, the spatial pattern is calculated by compositing by MJO phase. Only days with a strong MJO signal are considered (MJO amplitude has to exceed 1, see *Wheeler and Hendon*, [2004]). This selection process results in approximately 63% of the SPCZ labels being included (37% of SPCZ labels occur on days when there is not a strong MJO signal). Figure 8 shows the result of this composite in units of fraction of time present. Each panel is labeled with the MJO phase number, the location of enhanced MJO convection, and the number of days that were included in the composite.

[36] The propagation of the MJO signal within the SPCZ is quite clear. Both enhanced and suppressed convective signatures associated with the MJO are evident in SPCZ fraction of time present anomalies, and a distinct SPCZ spatial pattern is associated with each phase of the MJO. During MJO phases two and three the enhanced convection associated with the MJO is located over the Indian Ocean (outside the domain) and convection is suppressed north of Australia as is reflected in Figure 8. The absence of SPCZ activity north of Australia in MJO phase two becomes less pronounced in phase three. During MJO phases four and five, the MJO associated convection is located over the Maritime Continent, as reflected in increased SPCZ presence north of Australia. This enhanced SPCZ activity is not isolated to the tropics, but stretches southward to 30°S. The enhanced subtropical activity during these phases is confined between 160°E and 160°W. During MJO phases six and seven, the area where the SPCZ is more frequently present than normal expands eastward and poleward. Finally, during phases eight and one, there is again an absence of SPCZ north of Australia while the SPCZ is still more frequently present than normal over the central Pacific.

[37] SPCZ anomalies associated with an active MJO are not confined to the tropics but are seen as far south as 30°S. This is consistent with the analysis of a single case study

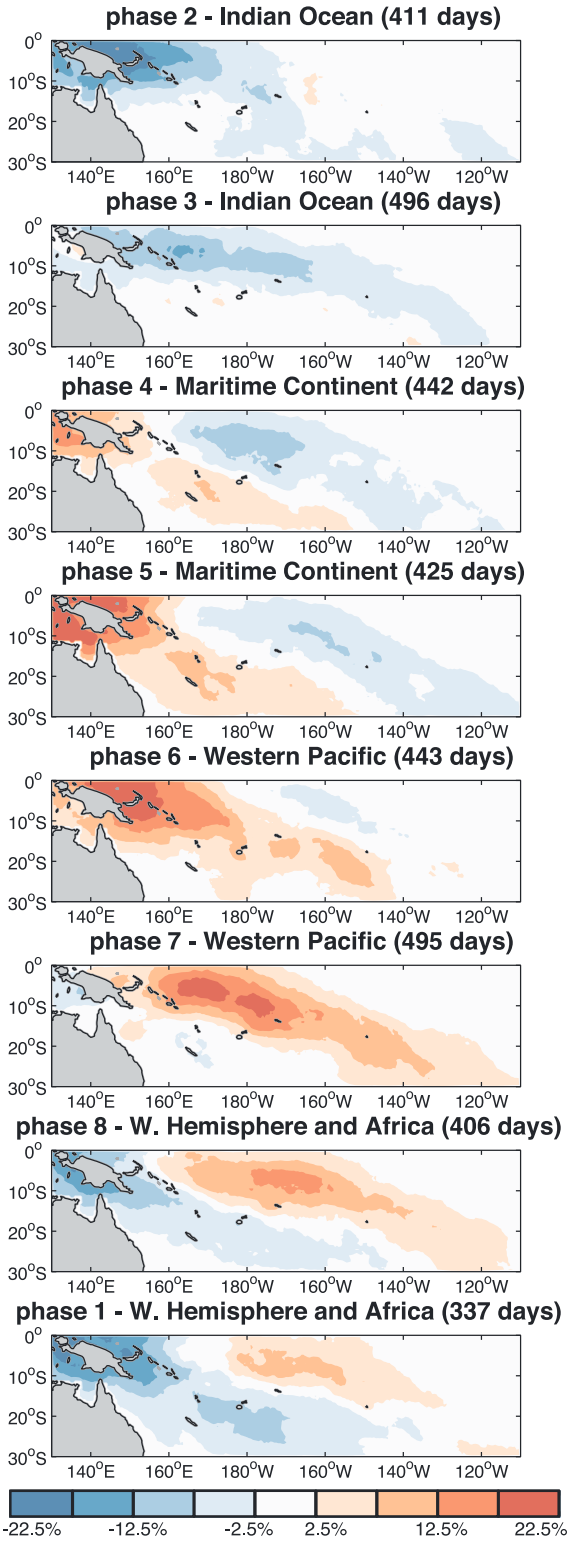

Figure 8. SPCZ fraction of time present anomalies (with respect to the average seasonal evolution) during each phase of the MJO. Phase based on the *Wheeler and Hendon* [2004] MJO index. Red shading indicates regions where the SPCZ is more frequently present than the mean, while blue shading indicates regions where the SPCZ is less frequently present than the mean. Titles indicate MJO phase number, location of enhanced convection associated with the MJO, and the number of days included in the composite.

during a strong MJO event in Mar–Apr 1988 by *Matthews et al*. [1996]. They note a poleward and eastward progression of low OLR (deep convection) along the SPCZ. Figure 8 shows the eastward progression of the pattern of enhanced convection associated with the propagation of the MJO in terms of 30 years of SPCZ activity.

4. Concluding Remarks

[38] A new and unique data set of SPCZ presence based on geostationary satellite observations has been used to quantify interannual and intraseasonal variability as well as the seasonal evolution of SPCZ location and extent over the past 30 years during the austral summer half-year (Nov–Apr). Our results suggest that two main axis lines describe the orientation of the SPCZ, one representing the more subtropical part in the southeast and another representing the tropical part in the northwest. In the subtropics the SPCZ is most active early in the season (Nov–Dec) when the SPCZ is present 30–40% of the time. SPCZ area in the subtropics peaks in late December. Studies that only consider the height of the SPCZ active season, which is typically defined as Dec–Feb, miss this activity in the subtropics in their analysis. We find that during the middle of the austral summer half-year, in Dec–Feb, the two axes of the mean SPCZ align to create one continuous convective region. During this time the SPCZ is frequently present in the tropics, 50–70% of the time, and SPCZ area in the tropics peaks in late January.

[39] The SPCZ is more constant and better defined in the tropics where the position and tilt align with the SST gradient. The warming of underlying SST in the subtropics during Jan–Mar does not directly affect SPCZ presence (as fraction of time present) and SPCZ area reaches a minimum in the subtropics in Jan–Mar. The latitudinal tilt in SPCZ presence is greater in the subtropics than the tilt of the warm SST pattern (Figure 5). Thus, the association of the subtropical SPCZ to seasonal changes in SST is different from that of the ITCZ in the tropical east Pacific, where ITCZ location is directly tied to the warmest SST [*Bain et al*., 2011]. The different behavior is directly tied to the different mechanisms for SPCZ maintenance in the subtropics, such as the role of the orography, the resulting subsidence, and dry air intrusion in organizing the tilt of the SPCZ [*Takahashi and Battisti*, 2007; *Lintner and Neelin*, 2008], and possible forcing from the Southern Hemispheric stormtrack [e.g., *Matthews*, 2012].

[40] We categorize each of the 30 seasons into a continuum of eight groups describing the dominant patterns of spatial variability of the SPCZ with no previous knowledge of ENSO mode. The resulting groups align with ENSO mode with some exceptions and this is broadly in agreement with *Vincent et al*. [2011], which defines four groups of interannual variability of the SPCZ. To summarize our results, during El Niño years, the SPCZ shifts to the north and east and the tropical portion takes on a more zonal orientation. During La Niña years, the SPCZ shifts south and west and the slope of the tropical portion becomes steeper. Previous studies did not have the means of examining the interannual variability in SPCZ area accompanying the shift in location. We find that despite the shifts in SPCZ location, there is no change in overall area associated with ENSO.

[41] We find a clear influence of the MJO in SPCZ location and extent on the intraseasonal time scale. We show the

detailed spatial pattern of SPCZ presence during each phase of the MJO, indicating the exact locations where SPCZ activity is enhanced and suppressed in each phase. Regions of enhanced SPCZ activity progress eastward with the propagation of MJO, and we find that the MJO can influence SPCZ activity throughout the domain, as far as 30°S.

[42] The instantaneous SPCZ presence labels allow the study of SPCZ behavior on shorter time scales than those discussed in this paper. For example, SPCZ area shows a clear diurnal cycle. The diurnal cycle in SPCZ area and cloud top height within the SPCZ is an interesting topic that is left for future work.

[43] **Acknowledgments.** The authors acknowledge Ken Knapp at NOAA's National Climatic Data Center for providing IR data from the GridSat database. We thank Caroline Bain and Padhraic Smyth for assistance with the spatiotemporal statistical model and for valuable comments during this research and Yi-Hui Wang and Collin Lawrence for help labeling 1 month of new data. We thank Andrew Lorrey and two anonymous reviewers for helpful comments. This research was supported by NSF grant AGS-1206120.

References

Bain, C. L., G. Magnusdottir, P. Smyth, and H. Stern (2010), Diurnal cycle of the Intertropical Convergence Zone in the east Pacific, *J. Geophys. Res.*, *115*, D23116, doi:10.1029/2010JD014835.

Bain, C. L., J. De Paz, J. Kramer, G. Magnusdottir, P. Smyth, H. Stern, and C. Wang (2011), Detecting the ITCZ in instantaneous satellite data using spatiotemporal statistical modeling: ITCZ climatology in the East Pacific, *J. Clim.*, *24*, 216–230, doi:10.1175/2010JCLI3716.1.

Diamond, H. J., A. M. Lorrey, and J. A. Renwick (2013), A southwest Pacific tropical cyclone climatology and linkages to the El Niño–Southern Oscillation, *J. Clim.*, *26*, 3–25, doi:10.1175/JCLI-D-12-00077.1.

Folland, C. K., J. A. Renwick, M. J. Salinger, and A. B. Mullan (2002), Relative influences of the interdecadal Pacific oscillation and ENSO on the South Pacific Convergence Zone, *Geophys. Res. Lett.*, *29*(*13*), 1643, doi:10.1029/2001GL014201.

Geman, S., and D. Geman (1984), Stochastic relaxation, Gibbs distribution and the Bayesian restoration of images, *IEEE Trans. Pattern Anal. Mach. Intell.*, *6*, 721–741.

Gilks, W., S. Richardson, and D. Spiegelhalter (1996), *Markov Chain Monte Carlo in Practice*, Chapman and Hall, Boca Raton, FL.

Gray, W. M. (1979), Hurricanes: Their formation, structure and likely role in the tropical circulation, *Meteorology Over Tropical Oceans*, *Roy. Meteor. Soc.*, edited by D. B. Shaw, pp. 155–218, Bracknell, England.

Henke, D., P. Smyth, C. Haffke, and G. Magnusdottir (2012), Automated analysis of the temporal behavior of the double Intertropical Convergence Zone over the east Pacific, *Rem. Sens. Environ.*, *123*, 418–433, doi:10.1016/j.rse.2012.03.022.

Jourdain, N. C., P. Marchesiello, C. E. Menkes, J. Lefèvre, E. M. Vincent, M. Lengaigne, and F. Chauvin (2011), Mesoscale simulation of tropical cyclones in the South Pacific: Climatology and interannual variability, *J. Clim.*, *24*, 3–25, doi:10.1175/2010JCLI3559.1.

Knapp, K., et al. (2011), Globally gridded satellite observations for climate studies, *Bull. Am. Meteorol. Soc.*, *92*, 893–907, doi:10.1175/2011BAMS3039.1.

Kodama, Y. M. (1999), Roles of the atmospheric heat sources in maintaining the subtropical convergence zones: An aqua-planet GCM study, *J. Atmos. Sci.*, *56*, 4,032–4,049.

Lintner, B. R., and J. D. Neelin (2008), Eastern margin variability of the South Pacific Convergence Zone, *Geophys. Res. Lett.*, *35*, L16701, doi:10.1029/2008GL034298.

Lorrey, A., G. Dalu, J. Renwick, H. Diamond, and M. Gaetani (2012), Reconstructing the South Pacific Convergence Zone position during the presatellite era: A La Niña case study, *Mon. Weather Rev.*, *140*, 3,653–3,668, doi:10.1175/MWR-D-11-00228.1.

Madden, R. A., and P. R. Julian (1993), Observations of the 40–50-day tropical oscillation: A review, *Mon. Weather Rev.*, *122*, 814–837.

Matthews, A. J. (2012), A multiscale framework for the origin and variability of the South Pacific Convergence Zone, *Q. J. R. Meteorol. Soc.*, *138*, 1,165–1,178, doi:10.1002/qj.1870.

Matthews, A. J., B. J. Hoskins, J. M. Slingo, and M. Blackburn (1996), Development of convection along the SPCZ within a Madden-Julian oscillation, *Q. J. R. Meteorol. Soc.*, *122*, 669–688.

Reynolds, R. W., N. A. Rayner, T. M. Smith, D. C. Stokes, and W. Wang (2002), An improved in situ and satellite SST analysis for climate, *J. Clim.*, *15*, 1609–1625.

Takahashi, K., and D. S. Battisti (2007), Processes controlling the mean tropical Pacific precipitation pattern. Part II: The SPCZ and the Southeast Pacific dry zone, *J. Clim.*, *20*, 5696–5706.

Vincent, D. G. (1994), The South Pacific Convergence Zone (SPCZ): A review, *Mon. Weather Rev.*, *122*, 1949–1970.

Vincent, E. M., M. Lengaigne, C. E. Menkes, N. C. Jourdain, P. Marchesiello, and G. Madec (2011), Interannual variability of the South Pacific Convergence Zone and implications for tropical cyclone genesis, *Clim. Dyn.*, *36*, 1881–1896, doi:10.1007/s00382-009-0716-3.

Wheeler, M. C., and H. H. Hendon (2004), An all-season real-time multivariate MJO index: Development of an index for monitoring and prediction, *Mon. Weather Rev.*, *132*, 1917–1932.

Widlanski, M. J., P. J. Webster, and C. D. Hoyos (2011), On the location and orientation of the South Pacific Convergence Zone, *Clim. Dyn.*, *36*, 561–578, doi:10.1007/s00382-010-0871-6.

Wolter, K., and M. S. Timlin (1998), Measuring the strength of ENSO events: How does 1997/98 rank?, *Weather*, *53*, 315–324.

Xie, S. -P. (2005), The shape of continents, air-sea interaction, and the rising branch of the Hadley circulation, in *The Hadley Circulation: Present, Past, and Future*, edited by H. F. Diaz and R. S. Bradley, pp. 121–152, Kluwer Academic Publishers, Netherlands.